Comparison of micro-structural snowpack parameters derived from penetration resistance measurements with fracture character observations from compression tests

Alec van Herwijnen *, Sascha Bellaire, Jürg Schweizer

WSL Institute for Snow and Avalanche Research SLF, Davos, Switzerland

ABSTRACT

Compression tests are snow stability tests that are widely used by avalanche professionals and snow researchers to identify potential weak snowpack layers. Describing fracture character in addition to the number of taps required to initiate a fracture improves the interpretation of compression test results, since certain types of fractures, i.e. sudden fractures, are more often associated with skier-triggered avalanches. Digital snowpack penetrometers provide high resolution penetration resistance data of the snow cover with depth. The SnowMicroPen (SMP) was used to measure high resolution penetration resistance profiles in the snowpack next to compression tests. A reliable method to automatically detect the snow surface in the SMP signals was introduced. Furthermore, a method based on the autocorrelation of the penetration resistance signal was developed to identify the failure layers, identified using compression tests, in the penetration resistance profiles. Using field data from 190 penetration resistance measurements, each collected between two compression tests, micro-structural parameters associated with different types of fractures were identified. More than 550 fractures were classified as either Progressive Compression (1.3%), Resistant Planar (12.1%), Sudden Planar (50.4%), Sudden Collapse (26.8%) or non-planar Break (9.4%). Measurement and analysis were focussed on micro-structural properties of the failure layer, the layer adjacent to the failure layer and the slab above the failure layer. Sudden collapse fractures were found to have typical micro-structural snowpack parameters that are generally associated with unstable snow conditions, such as large differences in penetration resistance between the failure layer and the adjacent layer.

© 2009 Elsevier B.V. All rights reserved.

1. Introduction

Snowpack data such as snow profiles and snow stability tests are often used for avalanche forecasting. The identification of potential weak layers within the snow cover is an important part of gathering these data and often relies on snow stability tests. The compression test is a snow stability test which is widely used by avalanche professionals and snow researchers to identify these potential weak layers (Canadian Avalanche Association, 2007).

It is well known that the frequency of skier-triggered dry snow slab avalanches decreases with increasing test score (Jamieson, 1999). It is also well established that the test score can be highly variable and is not the only result relevant for stability evaluation (Schweizer et al., 2008). Furthermore, there are often many failure layers observed in compression tests which are not failure planes in other stability tests such as the Rutschblock test (Winkler and Schweizer, 2009-this issue). The compression test usually identifies the failure layer in the Rutschblock test, but often many other layers as well. Additional

information about the character of the fracture can provide valuable information to interpret compression test results (Johnson and Birkeland, 2002; van Herwijnen and Jamieson, 2007).

The test score, i.e. the loading step at the moment of failure, relates to the strength of the weak layer. It therefore relates to fracture initiation, which is the first stage of avalanche release. The addition of a description of fracture character improves the interpretation of compression test results since certain types of fractures, i.e. sudden fractures, are more often associated with skier-triggered avalanches (van Herwijnen and Jamieson, 2007). Distinguishing between different types of fractures presumably provides information on fracture propagation, which is the second stage of avalanche release.

van Herwijnen and Jamieson (2007) showed that typical snowpack properties associated with sudden fractures favour skier-triggering, e.g. large hand hardness and crystal size differences between the failure layer and the adjacent layers. However, it is unclear why these snowpack properties favour sudden fractures since knowledge about the micro-mechanism of the various fractures is largely unknown.

Over the last decade, digital penetrometers have been developed to enable rapid, high resolution snowpack resistance measurements (e.g. Schneebeli and Johnson, 1998; Mackenzie and Payten, 2002). These

penetration resistance measurements can be used to derive micro-mechanical snowpack properties. However, measuring penetration resistance and determining micro-mechanical properties is influenced by the size and shape of the tip of the measurement instrument (Fukue, 1979; Johnson, 2003). For the SnowMicroPen (SMP), a digital penetrometer developed in Switzerland, Johnson and Schneebeli (1999) developed a model to derive micro-mechanical snow properties from the resistance measurements. When applied to measurements of snow properties, this model was able to determine compressive strength quite well but calculated values for elastic modulus were two orders of magnitude different from other measurements (Kronholm, 2004).

Previous studies using the SMP analysed properties of specific weak layers, such as surface hoar layers, in space and time using various statistical methods (e.g. Kronholm et al., 2004; Lutz et al., 2007). Pielmeier and Schweizer (2007) related snow layer properties derived from the SMP signal to snow cover stability. They found that failure layer hardness, differences in hardness between the failure layer and the adjacent layer, as well as the structural size (related to grain size), are indicators for unstable snowpack conditions.

Floyer and Jamieson (2009-this issue) used a modified version of the lower resolution SABRE penetrometer to identified weak layers associated with fractures in compression tests in penetrometer signals. When grouping fractures in compression tests as sudden and others (not sudden), they identified weak layer thickness, hardness gradient above the weak layer and hardness gradient below the weak layer as the variables offering the best discrimination between the two groups of fractures.

In this study we analyse compression test results performed next to high resolution penetration resistance measurements of the snow cover. The goal is to identify typical micro-structural snowpack parameters associated with different types of fractures in compression tests.

2. Methods

2.1. Field measurements

As part of a study on spatial variability of snow stability (Bellaire and Schweizer, in press), we performed 350 compression tests in 19 spatial grids around Davos, Switzerland, from January 2007 to April 2009. Fractures in compression tests were systematically classified using a five level description of fracture character (van Herwijnen and Jamieson, 2007): Progressive Compression (PC), Resistant Planar (RP), Sudden Planar (SP), Sudden Collapse (SC) and non-planar Break (B).

In the centre of each spatial grid a manual snow profile was observed giving us information such as grain shape, grain size (e) and hand hardness index (h) of each snow layer. Two compression tests were performed next to the manual snow profile. Two compression tests were also performed at 9 different locations throughout the grid within a distance of 30 cm of a SMP profile (Fig. 1). The SMP consists of a probe which is driven into the snow cover at a constant speed of 20 mm/s (Schneebeli and Johnson, 1998). Changes in hardness are recorded with a cone shaped tip with a diameter of 5 mm connected to a piezo-electric force sensor. The force sensor measures penetration resistance approximately every 4 μm, i.e. 250 measurements per mm. In total, 190 SMP profiles were measured and 380 compression tests were performed.

2.2. Snow surface detection

The first few centimeters of the SMP signal are recorded in the air as the tip of the probe moves towards the snow surface. In order to compare failure depths in the compression tests with layers within the SMP signal, an accurate detection of the snow surface is required. Usually, the snow-air interface is identified by hand, which is a time consuming endeavour. In order to automatically pick the snow surface, a signal processing method commonly used in seismology, the Akaike's
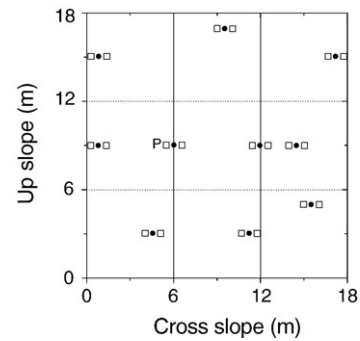

Fig. 1. Schematic representation of spatial grid measurement layout. The location of the manual profile is indicated with a P, SMP measurements by filled circles and compression tests by open squares.

Information Criterion (AIC), was applied to the SMP signal. The AIC function is based on the variance of the signal and is used to extract wave arrival times (e.g. Kurz et al., 2005).

The AIC function gives reliable onset picks only if the AIC is applied to the part of the signal containing the onset. Therefore, a rough estimate of the onset was determined by applying an empirical threshold of 0.05 N to the moving averaged penetration resistance signal, averaged over 1000 measurements (approximately 4 mm). The minimum in the AIC function of the raw SMP signal before the first crossing of the threshold determined the location of the snow surface.

2.3. Failure layer detection

SMP measurements have so far mainly been used to study the micro-mechanical properties of known failure layers (e.g. Pielmeier and Schweizer, 2007). The location of these layers in the SMP signal was visually identified based on an adjacent manual snow profile. However, if the location of the failure layer in the SMP profile is largely unknown, for example, when no manual snow profile is available, the identification of failure layers is not straightforward, since failure layers can be relatively thick and not much softer than the surrounding snow (e.g. Bellaire et al., 2009).

Failure layers in compression tests were first identified within the manually observed snow profile, which served as a reference. By comparing the snow profile with the SMP signal measured next to it, the failure layers were visually identified within this SMP signal (Fig. 2). In order to identify the failure layer in the remaining SMP signals, i.e. those 9 measurements not close to the profile location, a method was developed to automatically pick the failure layer. The method used proceeded as follows:

1. Smoothed SMP signals, denoted by S, were generated by taking the average over 25 points, corresponding to approximately 0.1 mm.
2. The decay in the correlation coefficient with lag distance of a moving window autocorrelation was determined for a 10 cm long section of the smoothed SMP signal ($S_{p,FL}$) centred around the middle of the manually identified failure layer at the profile location. The autocorrelation is a mathematical method for finding repeating patterns within a signal by correlating the signal with a shifted version of itself. A correlation coefficient is calculated for different shift distances, called lags. The decay in the correlation coefficient with lag distance indicates the degree of spatial homogeneity of the signal. The basis for using this method is that the decay of the autocorrelation should be relatively low within the failure layer and should increase at the interface with the adjacent layers. At every data point along the smoothed SMP signal $S_{p,FL}$ the exponential decay of the moving window autocorrelation was calculated for windows of 50 points (i.e. 5 mm windows). A suitable threshold value in the decay was visually determined to
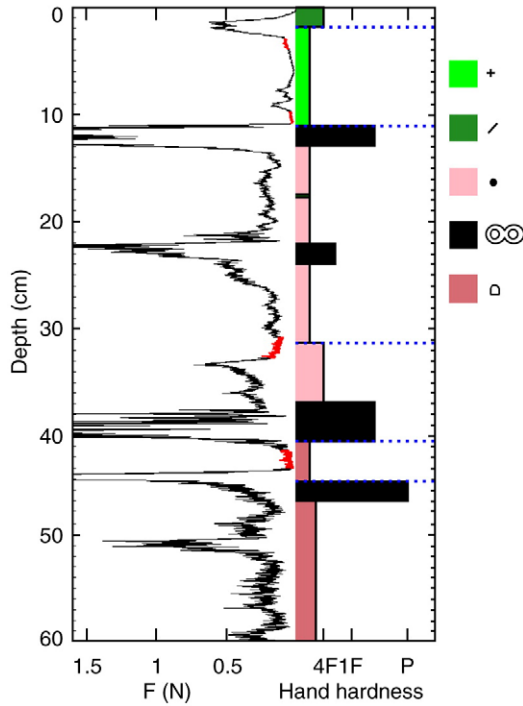
Fig. 2. Manual picking of failure layers was done in the SMP signal next to the manual snow profile. (left) SMP signal. (right) Hand hardness and crystal type of manual snow profile. The blue dashed lines indicate failures in compression tests and the red portions of the SMP signal the manually picked failure layers.

isolate the part of the signal coinciding with the failure layer at the profile location (Fig. 3).

3. A rough localization of the failure layer within the other SMP signals was obtained by cross-correlating $S_{\mathrm{p,FL}}$ with the mean SMP signal at the other locations in the grid. This was done by searching for a maximum in the cross-correlation of $S_{\mathrm{p,FL}}$ with a 20 cm portion of the SMP signals centred around the depth of the failure layer in the compression test at the different locations (Fig. 4a). For this step, it was assumed that the failure layer in the SMP profiles can be found within ± 10 cm of the failure in the nearby compression test.

4. The exact location of the failure layer was determined using the decay of the moving window autocorrelation of the portion of the signal which most closely matched $S_{\mathrm{p,FL}}$. By using the same threshold value for the decay of the autocorrelation as determined
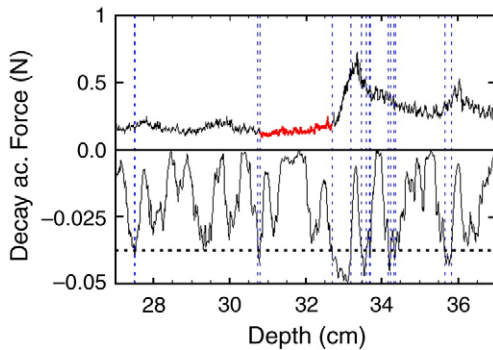
Fig. 3. A threshold value in the decay of the autocorrelation with lag distance was manually picked to isolate the part of the signal coinciding with the failure layer. (top) SMP signal and failure layer (red). (bottom) Decay in the autocorrelation function and threshold value (black dashed line). The blue dashed vertical lines indicate layer boundaries picked on the SMP signal.

at the profile location, the failure layer was automatically identified within the SMP signal (Fig. 4b).

In order to use this method, only failures in compression tests that were linked to layers observed in the snow profile could be used in the analysis, excluding 59 from the 628 recorded fractures.

2.4. Adjacent layer detection

The location of the layer adjacent to the failure layer, either the layer above or the layer below the failure layer, was determined in the field by examination of the fracture in the compression test and identified within the manual snow profile. Automatic detection of these layers within the SMP profiles was done using a method very similar to the one described above.

First, the location of the layer adjacent to the failure layer was visually identified at the profile location and a suitable threshold value in the decay of the autocorrelation was determined to isolate the part of the signal coinciding with the adjacent layer. Then, a rough localization of the adjacent layer within the other SMP signals was obtained by cross-correlating the manually identified adjacent layer at the profile location with the smoothed SMP signal at the other locations in the grid. This was done by searching for a maximum in the cross-correlation coefficient in the first 5 cm above the upper boundary of the failure layer for an adjacent layer above the failure layer and within the first 5 cm below the lower boundary for an adjacent layer below the failure layer. Finally, the exact location of the adjacent layer was determined using the decay of the moving window autocorrelation using the same threshold value for the decay of the autocorrelation as determined at the profile location.

The slab above the weak layer was defined as all layers above the failure layer. When the fracture in the compression test occurred at the top of the failure layer, the layer adjacent to the failure layer was included in the slab.

2.5. Micro-structural SMP parameters

Johnson and Schneebeli (1999) developed a micro-structural model to derive micro-mechanical properties of snow layers from the SMP signal. The micro-structural parameters derived from the penetration resistance signals used in this study are given in Table 1. The parameter Ψ is the product of the number of fractures per mm and the rupture force divided by the lateral area of the SMP tip (Bellaire et al., 2009):

$$\Psi = \frac{f_r n_{\mathrm{peaks}}}{A} \tag{1}$$

where f_r is the rupture force averaged over 1 mm, n_{peaks} is the number of peaks in the SMP signal over one mm and A is the lateral area of the sensor tip (~ 39 mm^2). The parameter Ψ is typically smaller for poorly bonded snow (e.g. depth hoar and surface hoar) than well bonded snow due to the much higher number of peaks in well bonded snow. This parameter has been used in a method to automatically detect the most critical weak layers within SMP signals (Bellaire et al., 2009).

The mean values of the parameters shown in Table 1 were derived for the failure layer (FL), the adjacent layer (AL) and for the slab (SL), as in Pielmeier and Schweizer (2007). Furthermore, relative differences in these parameters, denoted by Δ, between the failure layer and both the adjacent layer and the slab were calculated. For instance, the relative difference in mean force between the slab and the failure layer was calculated as:

$$\Delta \overline{F}_{\mathrm{SL-FL}} = \frac{\overline{F}_{\mathrm{SL}} - \overline{F}_{\mathrm{FL}}}{\overline{F}_{\mathrm{SL}}}. \tag{2}$$
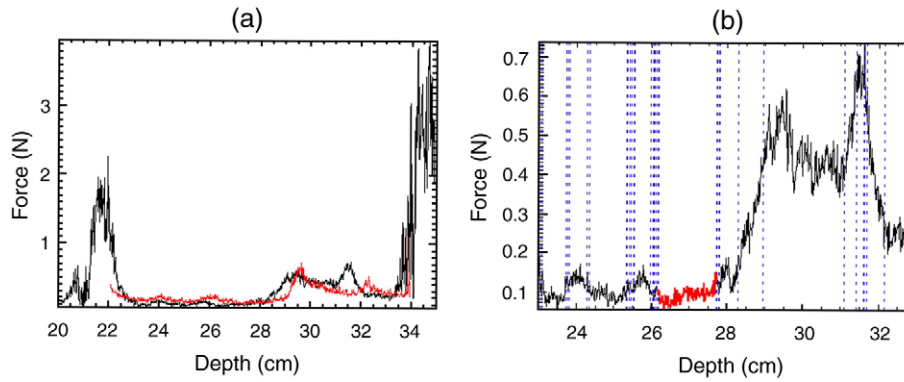
Fig. 4. (a) Best match between a SMP signal not taken at the profile location and the signal containing the manually picked failure layer from the profile location (red). (b) Automatic failure layer detection (red portion of the signal) based on the decay of the autocorrelation. The blue dashed vertical lines indicate layer boundaries picked on the SMP signal.

2.6. Statistical analysis

Non-parametric descriptors, e.g. median rather than mean, were used to characterize the distributions since the SMP signal is generally non-normally distributed (Kronholm et al., 2004; Lutz et al., 2007). To compare data we used the non-parametric Mann–Whitney U-test. Data were judged to be significantly different at a significance level of $p \leq 0.01$.

3. Results

3.1. Snow surface detection

In order to test the accuracy of the snow surface detection method based on the AIC criterion, we used a different dataset of 293 SMP signals for which the snow surface had been picked manually. In Fig. 5, the manually picked location of the snow surface is compared to the location of the automatically picked snow surface. There was a good accordance between manual and automatic snow surface picks. Eighty percent of the automatic snow surface picks were within 1 cm of the manually determined snow surface (RMS error of 2.6 cm). The remaining 20% of the SMP measurements were visually inspected by an experienced SMP user to determine the likely source of error in the automatically picked snow surface. In 8% of the cases where the difference between the manual and the automatic snow surface pick was greater than 1 cm, the automatically picked snow surface was deemed more accurate than the manual pick (triangles in Fig. 5). In 54% of the cases signal errors resulted in inaccurate automatic surface picking (squares) and in 38% of the cases the manually determined snow surface was considered more accurate (diamonds). These latter cases typically consisted of a soft layer of fresh snow on top of a harder layer (e.g. crust) and the automatically picked snow surface was then identified at the top of the harder layer below the real snow surface.

For the SMP data used in this study, the accuracy of the automatic detection of the snow surface was visually checked by displaying it on the SMP profile. In 77% of the cases, the automatically picked snow surface was considered to be in the right location. For the remaining 23% of the SMP profiles the location of the snow surface was manually identified.

### 3.2. Failure layer and adjacent layer detection

The accuracy of the methods used to automatically detect failure layers and layers adjacent to failure layers was also visually inspected by displaying the results on the SMP profiles. The position of 78% of the failure layers was considered as accurate while the accuracy of the automatic detection of the adjacent layers was somewhat lower with 69%. The falsely identified layers were not in the right location because the cross-correlated signals were not matched adequately. The maximum in the cross-correlation coefficient was significantly higher for the failure layers (median of 0.77) and the adjacent layers (median of 0.80) which were accurately detected than for the falsely identified failure layers (median of 0.63, $p<0.01$) and adjacent layers (median of 0.66, $p<0.01$). When the automatically identified layers were considered in the wrong location, the best match between the SMP signal from the profile location and the SMP signal under investigation was manually determined and the exact location of the layer was picked using the last step (point 4) in the method described in Section 2.3.

3.3. Snowpack characteristics and compression test results

The frequency of observation for each fracture type is given in Table 2. SP fractures were most often observed, followed by SC, RP, B and PC fractures. Since Sudden Planar fractures were most common in our data set, we used these as a reference to compare data from other fracture types with. There were only 7 recorded PC fractures in our

Table 1
Micro-structural parameters derived from the penetration resistance measurement.

Parameter	Description
F (N)	Mean penetration resistance
n_{peaks} (mm^{-1})	Number of peaks per mm
L_n (mm)	Element length
f_r (N)	Rupture force
E (kPa)	Macro mechanical elastic modulus
Σ (kPa)	Macro mechanical compactive strength
Ψ (kPa)	Parameter described by Bellaire et al. (2009)
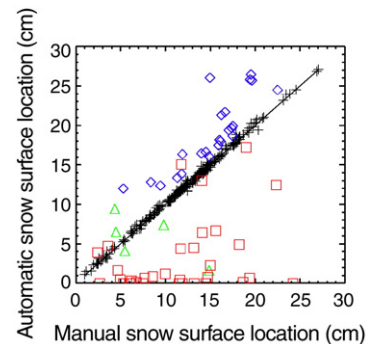
Fig. 5. Comparison between manual and automatic snow surface picking. The solid line indicates the one-to-one relationship. Black crosses indicate differences in snow surface picking less than 1 cm. Difference in snow surface picking larger than 1 cm are highlighted: diamonds indicate signals where the manual snow surface picking was more accurate, triangles indicate more accurate automatic picking and squares indicate inaccurate automatic picking due to signal errors.

Table 2

Number of observations and frequency of observation for each category of fracture character.

Fracture character	N	Frequency (%)
PC	7	1.3
RP	67	12.1
SP	278	50.4
SC	148	26.8
B	52	9.4

Fig. 6. Percentage of failure layer grain type by fracture character. Failure layer grain types were grouped as new snow (PP/DF), rounded grains (RG), faceted crystals (FC), depth hoar (DH) and surface hoar (SH). The numbers indicate the total number of observations for each fracture type.

data. Previous work has shown that PC and RP fractures are typically associated with fairly similar snowpack conditions (van Herwijnen and Jamieson, 2007). Therefore, we grouped both fracture types in one category.

A summary of compression test results and snowpack characteristics observed in the manual snow profile is shown in Table 3 for each fracture type. While the differences in the median value of the parameters were rather small, there were some significant differences. Most parameters associated with PC/RP fractures were significantly different from those associated with SP fractures. Compared to SP fractures, PC/RP fractures were typically associated with shallower, softer slabs and the differences in hand hardness and crystal size between the failure layer and the slab were significantly smaller. Likewise, almost all parameters associated with SC fractures were significantly different from those associated with SP fractures. Sudden collapse fractures were typically associated with deeper, harder slabs and required more taps to fracture compared to SP fractures. Furthermore, the failure layers associated with SC fractures were typically softer and composed of larger crystals than failure layers associated with SP fractures. The differences in hardness and grain size between the failure layer and both the adjacent layer and the slab were significantly larger. Finally, most variables associated with non-planar breaks (B) showed little differences with those associated with SP fractures.
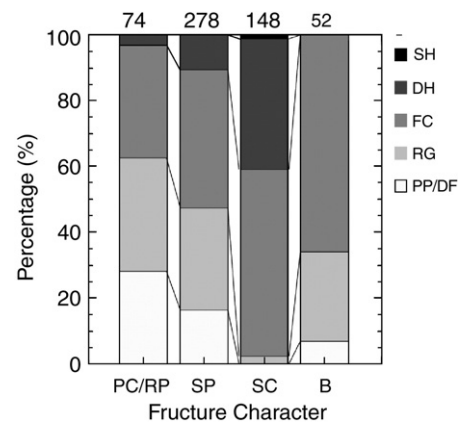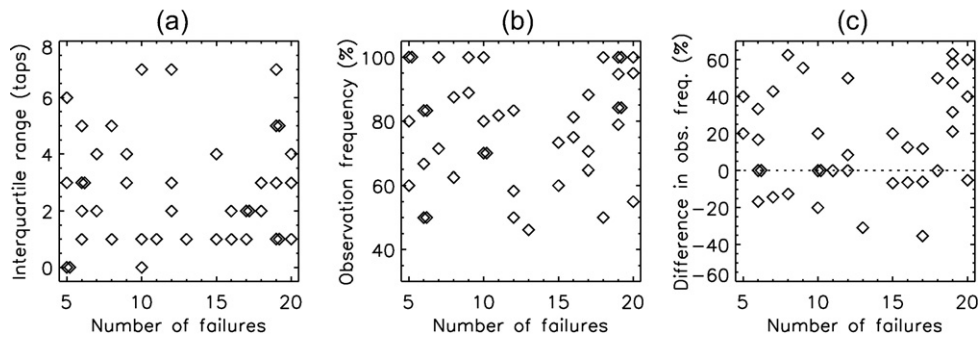
The distribution of failure layer grain type for each fracture type is shown in Fig. 6. Failure layer grain type was classified as new snow (PP/DF; i.e. layers composed of precipitation particles or decomposing and fragmented particles), rounded grains (RG), faceted crystals (FC), depth hoar (DH) and surface hoar (SH). Most PC/RP fractures were associated with failure layers composed of non-persistent failure layers (i.e. PP/DF and RG) while the majority of SC and B fractures were associated with persistent failure layers (FC, DH and SH). Approximately as many non-persistent failure layers (47%) as persistent failure layers (53%) were associated with SP fractures.

3.4. Variability of compression test results and fracture character observations

In the compression tests, all 552 failures were associated with 58 different failure layers. Each failure layer was not necessarily associated with a failure in each compression test. The maximum number of possible failures for one failure layer throughout a measurement grid was 20, i.e. two compression tests next to the manual snow profile and two compression tests at nine different locations. The median number of failures per failure layer was 9 (first and third quartile of 3 and 16, respectively). In 5 out of 58 cases (9%) the failure layer was associated with failures in all the compression tests (i.e. 20 failures) and in 7 out of 58 cases (12%) was the failure layer associated with only one failure in the compression tests throughout the measurement grid.

The compression test score and fracture character observations varied for most failure layers throughout the measurement grid. In order to quantify the variability in these observables, only layers which were associated with at least five failures in the compression tests (i.e. in at least 25% of the compression tests) were considered, excluding 16 of the 58 failure layers.

To quantify the variability in compression test score the interquartile range of the compression test score, i.e. the range comprising the middle 50% of the data, was determined for each failure layer associated with at least 5 failures in compression tests (Fig. 7a). The median interquartile range of the compression test score was 2 taps

Table 3

Descriptive statistics for compression test results and manually observed snowpack properties for each fracture character, showing the median (Med), the first quartile (Q1) and third quartile (Q3).

Parameter	Fracture character											
	PC/RP			SP			SC			B		
	Q1	Med	Q3	Q1	Med	Q3	Q1	Med	Q3	Q1	Med	Q3
Depth (cm)	**13**	**18**	**28**	23	34	45	**38**	**47**	**72**	22	29	48
Taps	11	13	16	12	13	17	**13**	**16**	**20**	12	14	19
h_{FL}	1	1	1.5	1	1	1.5	**1**	**1**	**1**	1	1.5	1.5
e_{FL} (mm)	**0.5**	**0.5**	**0.75**	0.5	1	1	**1**	**1.5**	**2**	0.5	1	1.5
h_{AD}	2	2.5	3	2	2.5	3.5	2	2.5	3.5	2	3	3.5
e_{AD} (mm)	0.5	0.5	0.5	0.5	0.5	0.5	**0.5**	**0.75**	**1**	**0.5**	**0.5**	**0.75**
h_{SL}	**1.2**	**1.6**	**1.7**	1.5	1.6	2.1	**1.7**	**1.9**	**2.2**	1.5	1.9	2.2
e_{SL} (mm)	**0.5**	**0.6**	**0.7**	0.4	0.5	0.6	0.5	0.5	0.6	**0.5**	**0.6**	**0.8**
$h_{AD} - h_{FL}$	0.5	1	1.5	1	1	1.5	**1**	**1.5**	**2**	0.5	1.5	2
$e_{FL} - e_{AD}$ (mm)	**0**	**0**	**0.25**	0	0.25	0.5	**0.5**	**1**	**1**	0	0	0.75
$h_{SL} - h_{FL}$	**0**	**0.2**	**0.5**	0	0.5	0.7	**0.6**	**0.7**	**1.2**	0.4	0.6	0.7
$e_{FL} - e_{SL}$ (mm)	**−0.16**	**0.02**	**0.12**	0.06	0.25	0.7	**0.56**	**0.75**	**1.48**	−0.04	0.26	0.71

Parameters that were significantly different from those of SP fractures are indicated in bold. The depth of the failure in the compression test, the number of taps at failure, the hand hardness index (h) and the grain size (e) are shown for the failure layer (FL), the adjacent layer (AL) and the slab (SL). Differences in hand hardness index and grain size are also shown.

Fig. 7. Variability of compression test score and fracture character observations for failure layers associated with at least 5 failures in compression tests. (a) Interquartile range of the compression test score. (b) Observation frequency of the most commonly observed fracture type. (c) Difference in observation frequency of the most common fracture type and the observation frequency of compression test scores within ±1 taps of the median compression test score. The dashed line indicates zero difference.

(first and third quartile of 1 and 4 taps, respectively), meaning that typically 50% of the compression test results were within a range of 2 taps. As can be seen in Fig. 7a, the interquartile range showed no dependence on the number of fractures associated with the failure layer. The largest observed interquartile range was 7 taps for three failure layers associated with 10, 12 and 19 failures, respectively, while the lowest interquartile range was 0 taps for three failure layers associated with 5, 5 and 10 failures, respectively.

The variability of fracture character was quantified by determining the observation frequency of the most commonly observed fracture type associated with each failure layer (Fig. 7b). For failure layers which were associated with at least 5 failures in compression tests, SP was the most common fracture type for 24 of the 42 cases (i.e. 57%), followed by SC (24%), PC/RP (14%) and B (5%). The median observation frequency for the most common fracture type was 81% (first and third quartile of 65 and 95%, respectively). As with the interquartile range of the compression test score, the observation frequency showed no dependence on the number of fractures associated with the failure layer. For 9 failure layers the fracture character was the same for all failures observed in compression tests and in one case four fracture types were observed in failures associated with one failure layer.

In order to compare the variability of both these observables the difference between the observation frequency of the most common fracture type and the observation frequency of compression test scores within ±1 tap of the median compression test score was determined for each failure layer associated with at least 5 failures in compression tests (Fig. 7c). The tolerance of ±1 tap from the median is arbitrary but reasonable given the fact that the median interquartile range of the compression test score was 2 taps. The difference in observation frequency was positive in 25 out of 42 cases (i.e. 60%), meaning that in 60% of the cases fracture character was less variable than compression test score. In 24% of the cases compression test score was less variable (i.e. negative difference in observation frequency).

3.5. Micro-structural layer properties

The results from the statistical comparison of micro-structural parameters and fracture character for the failure layer, the adjacent layer and the slab are shown in Table 4. The micro-structural parameters of the failure layers and the adjacent layers associated with non-planar Breaks (B) showed no significant differences with those from SP fractures. For the slab, on the other hand, the rupture force, the elastic modulus, the compressive strength and Ψ were significantly larger for B fractures compared to SP fractures. All parameters associated with PC/RP fractures were significantly different from those associated with SP fractures. Failure layers, adjacent layers and slabs associated with PC/RP fractures generally had lower penetration resistance, number of peaks, rupture force, elastic modulus, compressive strength and Ψ parameter. The element length, on the other hand, was significantly larger. For SC fractures, all the parameters associated with the failure layer were significantly different from those associated with SP fractures, while very few adjacent layer parameters and no slab parameters were significantly different.

The distributions of the mean penetration resistance of the failure layer, the number of fractures per mm for the adjacent layer and the Ψ parameter for the slab are shown in Fig. 8. Clearly PC/RP fractures and SC fractures were typically associated with failure layers with a lower penetration resistance (Fig. 8a). As seen in Fig. 8b, adjacent layers associated with PC/RP and SC fractures had a lower median number of fractures per mm than adjacent layers associated with SP and B fracture types. Finally, the median value of Ψ_{SL} was lowest for RP fractures and highest for B fractures (Fig. 8c).

### 3.6. Relative micro-structural layer properties

The results from the statistical comparison of micro-structural parameters and fracture character for the relative difference between the adjacent layer and the failure layer as well as between the slab and

Table 4
Median values of the penetration resistance F, number of peaks per mm n_{peaks}, element length L_n, rupture force f_r, elastic modulus E, compressive strength Σ and parameter Ψ for each fracture type, for failure layer, adjacent layer, and slab layer.

Parameter	Failure layer				Adjacent layer				Slab			
	SP	SC	B	PC/RP	SP	SC	B	PC/RP	SP	SC	B	PC/RP
F (N)	0.08	**0.05**	0.10	**0.04**	0.46	0.39	0.49	**0.18**	0.21	0.12	0.32	**0.05**
n_{peaks} (mm^{-1})	9.9	**6.9**	13.1	**4.0**	36.1	**32.3**	39.9	**24.4**	15.0	10.6	16.1	**4.6**
L_n (mm)	1.5	**1.6**	1.5	**2.1**	0.9	0.9	0.9	**1.1**	1.3	1.5	1.2	**1.9**
f_r (N)	0.03	**0.04**	0.04	**0.02**	0.05	0.06	0.07	**0.04**	0.06	0.05	**0.07**	**0.03**
E (kPa)	8.2	8.5	13.0	**4.2**	43.1	51.8	54.0	**2.0**	24.8	15.6	**34.9**	6.3
Σ (kPa)	1.0	**1.3**	1.4	**0.8**	2.0	**2.6**	2.6	**1.5**	1.4	1.2	**1.6**	0.9
Ψ (kPa)	7.2	6.6	11.3	**2.6**	49.9	55.9	65.7	**22.6**	22.7	12.7	**34.2**	4.7

Variables that were significantly different from those associated with SP are marked in bold.
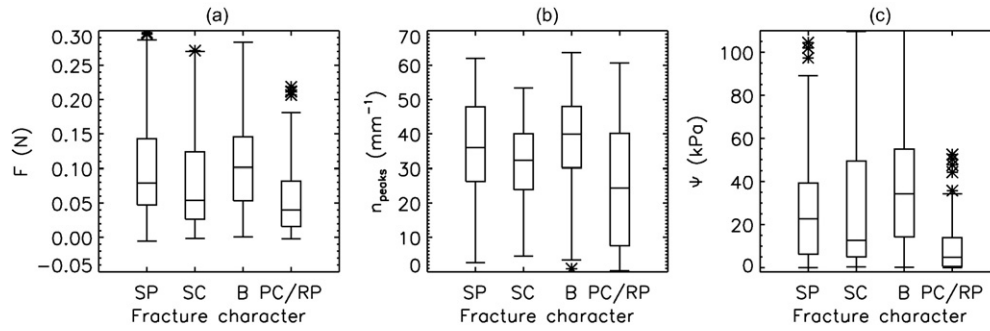
Fig. 8. Distribution of (a) mean penetration resistance of the failure layer, (b) number of fractures per mm of the adjacent layer and (c) Ψ parameter of the slab for each fracture type. The horizontal lines indicate the median value, the boxes indicate the interquartile range and the whiskers show the largest non-outlier range. Outliers are shown by asterisks.

the failure layer are shown in Table 5. Again, no significant differences were observed between SP and B fractures. The majority of the parameters associated with SC fractures were significantly larger than those associated with SP fractures. PC/RP fractures, on the other hand, were associated with significantly smaller values of $\Delta F_{SL–FL}$, $\Delta n_{peaks\ SL–FL}$, $\Delta L_{n\ FL–SL}$, $\Delta E_{SL–FL}$ and $\Delta \Psi_{SL–FL}$ than SP fractures.

The distribution of the relative differences in mean penetration resistance between the adjacent layer and the failure layer, and the relative differences in structural length between the slab and the failure layer are shown in Fig. 9. Sudden collapse fractures were clearly associated with larger relative differences in penetration resistance between the failure layer and the adjacent layer than SP fractures, while this was not the case for B and PC/RP fractures (Fig. 9a). Despite similar median values the distribution of $\Delta F_{AD–FL}$ for PC/RP fractures was skewed towards lower values compared to SP fractures. As can be seen in Fig. 9b, the relative difference in element length between the failure layer and the slab was lowest for PC/RP fractures and highest for SC fractures.

4. Discussion

The method used to automatically determine the snow surface was effective for determining the snow surface in high quality signals (Fig. 5). This method performed very well when the snow surface was relatively hard. However, the method failed to pick the snow surface correctly if the snowpack consisted of a few cm of very soft snow overlying a harder layer. This was due to the static threshold value of

0.05 N which was used to isolate the portion of the signal containing the snow surface before pinpointing the snow surface with the AIC criterion. Since very soft snow has very low penetration resistance, often less than 0.05 N, the harder layer beneath the snow surface was included in the rough estimate of the snow surface, causing the AIC criterion to pick the snow surface at the top of the harder layer. Employing a more adaptive threshold value, depending on signal quality and snow surface conditions might resolve this issue. Finally, when the signal-to-noise ratio of the signal in the air was large, e.g. due to signal drift or a defective coaxial cable, the snow surface was not accurately picked. Manual picking of the snow surface was then still required.

Using the method based on the cross-correlation and the auto-correlation of signals to automatically identify failure layers was reasonable successful. It required the manual picking of reference layers from the SMP signal measured at the location of the manually observed snow profile. Furthermore, this method required low spatial variability of the SMP signals evidenced by the significantly lower maximum in the cross-correlation coefficient of the falsely identified failure layers in SMP profiles than for failure layers which were considered as accurate (Section 3.2). Floyer and Jamieson (2008) employed a similar method based on a spiking deconvolution algorithm for tracing weak layers between penetrometer profiles across a grid of profiles. Their method also required pre-identification of the weak layer of interest. Nevertheless, while further development is required, such methods could potentially be used to automatically identify layer boundaries within penetrometer signals, which would greatly improve and facilitate the analysis and interpretation of these signals.

The data analysed here were collected for a study on spatial variability of snow stability (Bellaire and Schweizer, in press). The data show that compression test score and fracture character observations varied for most failure layers throughout the measurement grids. It has been proposed that fracture character should show less variability than test scores, although this has not yet been shown (Schweizer et al., 2008). Comparison of the variability of fracture

Table 5
Median values of relative differences of micro-structural parameters between the adjacent layer and the failure layer as well as between the slab and the failure layer.

Parameter	Fracture character			
	SP	SC	B	PC/RP
Adjacent layer and failure layer				
$\Delta F_{AL–FL}$	0.81	**0.89**	0.82	0.80
$\Delta n_{peaks\ AL–FL}$	0.66	**0.75**	0.65	0.75
$\Delta L_{nFL–AL}$	0.36	**0.41**	0.35	0.42
$\Delta f_{r\ AL–FL}$	0.41	0.41	0.39	0.41
$\Delta E_{AL–FL}$	0.79	**0.86**	0.75	0.82
$\Delta \Sigma_{AL–FL}$	0.43	0.48	0.43	0.42
$\Delta \Psi_{AL–FL}$	0.84	**0.90**	0.82	0.86
Slab and failure layer				
$\Delta F_{SL–FL}$	0.55	**0.66**	0.64	**0.40**
$\Delta n_{peaks\ SL–FL}$	0.21	**0.40**	0.32	**−0.18**
$\Delta L_{nFL–SL}$	0.11	**0.18**	0.15	**−0.02**
$\Delta f_{r\ SL–FL}$	0.30	**0.19**	0.43	0.27
$\Delta E_{SL–FL}$	0.45	0.48	0.60	**0.11**
$\Delta \Sigma_{SL–FL}$	0.08	**0.02**	0.27	0.15
$\Delta \Psi_{SL–FL}$	0.49	0.53	0.63	**0.09**

Variables that were significantly different from those associated with SP are marked in bold.
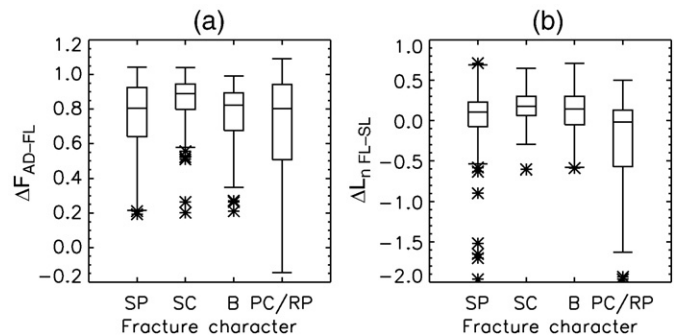
Fig. 9. Distribution of (a) the relative difference in mean penetration resistance between the adjacent layer and the failure layer and (b) the relative difference in element length between the failure layer and the slab for each fracture type. Symbols as in Fig. 8.

character observations with the variability of compression test score is not trivial since categorical data (i.e. fracture character) is compared with ordinal data (i.e. compression test score). Nevertheless, the data presented here suggest that fracture character is less variable than compression test score when using a tolerance of ± 1 tap from the median compression test score (Fig. 7c).

Even though there were over 550 recorded fractures, the data were only collected on 19 individual days and all the failures in compression tests were associated with only 58 different failure layers. Therefore, snowpack conditions were not very diverse, as indicated by the rather small differences in typical snowpack parameters associated with fracture character (Table 3). Field measurements of hand hardness can be thought of as a rough penetration resistance measurement (Pielmeier and Schneebeli, 2003), while grain size can be related to element length, although not for all grain types (Kronholm, 2004). Regarded in such a manner, the typical micro-structural snowpack parameters associated with fracture character (Tables 4 and 5) can be compared to typical manual snow profile parameters associated with fracture character identified by van Herwijnen and Jamieson (2007) for a much larger data set.

PC and RP fractures were typically associated with failure layers with low penetration resistance, large element length, low number of peaks per mm and low rupture force (Table 4). This is consistent with previous findings which showed that PC and RP fractures are typically associated with soft failure layers consisting of precipitation particles (i.e. large L_n and low n_{peaks} and f_r). Furthermore, even though ΔF_{AL-FL} and $\Delta L_{n\ FL-AL}$ were not significantly different from SP fractures, the differences between the failure layer and the slab were significantly smaller (Table 5). This is reasonably consistent with the small differences in hand hardness and grain size reported in van Herwijnen and Jamieson (2007).

Similarly to PC and RP fractures, SC fractures were generally associated with failure layers with low F, low n_{peaks} and large L_n. However, f_r was typically large (Table 4). This comes as no surprise since SC fractures are typically associated with persistent weak layers (van Herwijnen and Jamieson, 2007), for which the rupture force is generally higher than for new snow layers. Furthermore, failure layers associated with SC fractures generally had large relative differences in penetration resistance and element length between the failure layer and both the adjacent layer and the slab (Table 5). This agrees well with previous findings which showed that failure layers associated with SC fractures typically have large differences in hand hardness and crystal size compared to the adjacent layer.

Micro-structural snowpack parameters for SP and B fractures were very similar (Table 4 and 5), which was also the case for most manual snow profile parameters (van Herwijnen and Jamieson, 2007). However, there was no significant difference in ΔF_{AL-FL} and $\Delta L_{n\ FL-AL}$ between SP and B fractures, contrary to the results from van Herwijnen and Jamieson (2007) who found that SP factures were associated with failure layers with significantly larger hand hardness and crystal size differences compared to B fractures.

A study on the micro-structural parameters associated with stable and unstable snow profiles (Pielmeier and Schweizer, 2007) revealed that unstable snowpack layers typically have a low mean penetration resistance, significantly lower than the adjacent layer. Furthermore, unstable snowpack layers generally have a large mean element length and a low number of peaks, significantly lower than the adjacent layer. The results presented in this study show that sudden collapse fractures have typical micro-structural snowpack parameters which are generally associated with unstable snow conditions: low F, large L_n, large ΔF_{AL-FL}, large ΔF_{SL-FL}, large $\Delta L_{n\ FL-AL}$ and large $\Delta L_{n\ FL-SL}$ (Tables 4 and 5). This was not the case for SP fractures, which are also typically associated with skier-triggering. PC and RP fractures, which are generally not associated with skier-triggered avalanches, were typically associated with lower values of ΔF_{SL-FL} and $\Delta L_{n\ FL-SL}$. However, the differences in penetration resistance and element length

between the failure layer and the adjacent layer were not small (Table 5). Therefore, it is crucial that more data with a wider range of snowpack conditions are collected and analysed to determine the validity of the findings presented here.

Using a multivariate classification tree, we tried to identify variables to discriminate between different fracture types. However, splitting variables and the associated splitting values were not robust and the results from this analysis were deemed unreliable. This was attributed to the unbalanced data set (i.e. predominantly SP fractures), the high correlation between the micro-structural variables and the large overlap between the data in each fracture character classification. Using a linear discriminant analysis, Floyer and Jamieson (2009-this issue) reported good separation between sudden fractures and other fractures based on weak layer thickness, hardness gradient above the weak layer and hardness gradient below the weak layer, with a classification rate of 80%. However, this method was not successful when trying to separate individual fracture types, with a classification rate of only 37%. They suggested that given their measurements and analysis techniques, separation into each fracture character was not possible.

Using a high-speed camera van Herwijnen and Jamieson (2005) observed the physical processes associated with PC, RP, SP and SC fractures. For PC fractures the crystals in the failure layer were re-arranged after each loading step, RP fractures were characterized by the rearrangement of the crystals at the interface between the failure layer and the adjacent layer, SC fractures resulted from the extensive rearrangement of the crystals throughout the failure layer and SP fractures appeared to occur due to rupturing of the bonds between the failure layer and the adjacent layer. These observations suggest that, the compressive strength of the failure layer is of importance in particular for PC, RP and SC fractures. The compressive strength of failure layers associated with PC and RP fractures was typically low (Table 4), in good agreement with these observations. Furthermore, the compressive strength of the adjacent layers and slabs associated with PC and RP fractures were also generally low, suggesting that these layers could be involved in the fracture process, as proposed by van Herwijnen and Jamieson (2005). The compressive strength of layers that exhibited SC fractures, on the other hand, was typically high. While this might seem to contradict the observation of the failure process described above, it has to be noted that SC fractures are generally associated with persistent weak layers composed of facets or depth hoar (Fig. 6). Due to their anisotropic structure, layers of facets and depth hoar typically have a compressive strength which is higher than for fine grained snow (Akitaya, 1974), which explains the higher values of Σ associated with SC fractures.

5. Conclusions

One hundred and ninety SMP penetrometer measurements each performed in combination with two nearby compression tests were analysed in order to identify typical micro-structural snowpack parameters associated with fracture character. In order to extract micro-structural parameters from the SMP signals relating to fracture character, a method was introduced to automatically locate the snow surface in the SMP signal. Furthermore, a method was developed to automatically identify failure layers within the penetrometer signal.

The method for automatically identifying the snow surface, based on the AIC criterion of the signal, was effective and reliable, provided the penetrometer signal had few signal errors. Automatic identification of failure layers within penetrometer signals required manual picking of a reference layer from the SMP signal measured at the location of the manually observed snow profile. This method is therefore only suitable for use with multiple SMP measurements that show slight variations, such as in spatial grids or across transects. Nevertheless, with further development, this method could potentially be used to automatically

identify layer boundaries within penetrometer signals, an enhancement which would likely increase the practical use of penetrometers.

Data from over 550 failures in compression tests were collected on 19 individual days and the failures in compression tests were associated with 58 different failure layers. The data show that fracture character observations and compression test score varied for most failure layers. Comparison of the variability of compression test score and fracture character observations suggest that fracture character is less variable than compression test score when using a tolerance of ±1 tap from the median compression test score.

Despite the fact that snowpack conditions in the data were not very diverse, the comparison of micro-structural snowpack parameters with fracture character showed that sudden collapse fractures generally had micro-structural parameters associated with unstable snow conditions. Sudden collapse fractures were typically associated with large relative differences in element length and penetration resistance between the failure layer and both the slab and the adjacent layer. Progressive collapse and resistant planar fractures, on the other hand, were typically associated with smaller relative differences in element length and penetration resistance between the failure layer and the slab. However, this was not the case for the differences in penetration resistance and element length between the failure layer and the adjacent layer. Furthermore, few significant differences were observed between typical micro-structural snowpack parameters associated with B fractures and SP fractures. In order to determine the validity of these findings, more varied data are required.

Acknowledgements

References

Akitaya, E., 1974. Studies on depth hoar. Contrib. Inst. Low Temp. Sci., Ser. A 26, 1–67.

Bellaire, S., Schweizer, J., in press. Estimating slope stability from spatial snow cover observations. Cold Reg. Sci. Technol.

Bellaire, S., Pielmeier C., Schneebeli, M., Schweizer, J., 2009. Stability algorithm for snow micro penetrometer measurements. J. Glaciol. 55, (193).

Canadian Avalanche Association, 2007. Observation Guidelines and Recording Standards for Weather, Snowpack and Avalanches. Canadian Avalanche Association, Revelstoke, Canada.

Floyer, J.A., Jamieson, J.B., 2008. Avalanche weak layers traving and detection in snow penetrometer profiles. Proceedings of the 4th Canadian Conference on Geohazards, Quebec City, Canada, pp. 161–168.

Floyer, J.A., Jamieson, J.B., 2009. Predicting the fracture character of weak layers from snowpack penetrometer signals. Cold Reg. Sci. Technol. 59, 185–192 (this issue).

Fukue, M., 1979. Mechanical Performance of Snow Under Loading. Tokai University Press, Tokyo, Japan. 136 pp.

Jamieson, J.B., 1999. The compression test — after 25 years. Avalanche Rev. 18 (1), 10–12.

Johnson, J.B., 2003. A statistical micromechanical theory of cone penetration in granular materials. Report ERDC/CRREL-TR-03-3. U.S. Army Corps of Engineers, Engineer Research and Development Center, Hanover NH, U.S.A.

Johnson, J.B., Schneebeli, M., 1999. Characterizing the microstructural and micromechanical properties of snow. Cold Reg. Sci. Technol. 30 (1–3), 91–100.

Johnson, R.F., Birkeland, K.W., 2002. Integrating Shear Quality into Stability Test Results. Proceedings of the 2002 International Snow Science Workshop, Penticton, Canada, pp. 508–513.

Kronholm, K., 2004. Spatial variability of snow mechanical properties with regard to avalanche formation. Ph.D. thesis, University of Zürich, Zürich, Switzerland, 158 pp.

Kronholm, K., Schneebeli, M., Schweizer, J., 2004. Spatial variability of micropenetration resistance in snow layers on a small slope. Ann. Glaciol. 38, 202–208.

Kurz, J.H., Grosse, C.U., Reinhardt, H.W., 2005. Strategies for reliable automatic onset time picking of acoustic emissions and of ultrasound signals in concrete. Ultrasonics 43, 538–546.

Lutz, E., Birkeland, K.W., Kronholm, K., Hansen, K., Aspinall, R., 2007. Surface hoar characteristices derived from a snow micropenetrometer using moving window statistical operations. Cold Reg. Sci. Technol. 47 (1–2), 118–133.

Mackenzie, R., Payten, W., 2002. A Portable, Variable-Speed, Penetrometer for Snow Pit Evaluation, Proceedings of the 2002 International Snow Science Workshop, Penticton, Canada, pp. 294–300.

Pielmeier, C., Schneebeli, M., 2003. Stratigraphy and changes in hardness of snow measured by hand, ramsonde and snow micro penetrometer: a comparison with planar sections. Cold Reg. Sci. Technol. 37 (3), 393–405.

Pielmeier, C., Schweizer, J., 2007. Snowpack stability information derived from the SnowMicroPen signal. Cold Reg. Sci. Technol. 47 (1–2), 102–107.

Schneebeli, M., Johnson, J.B., 1998. A constant-speed penetrometer for high-resolution snow stratigraphy. Ann. Glaciol. 26, 107–111.

Schweizer, J, Kronholm, K., Jamieson, J.B., Birkeland, K.W., 2008. Review of spatial variability of snowpack properties and its importance for avalanche formation. Cold Reg. Sci. Technol. 51 (2–3), 253–272.

van Herwijnen, A., Jamieson, B., 2005. High-speed photography of fractures in weak snowpack layers. Cold Reg. Sci. Technol. 43 (1–2), 71–82.

van Herwijnen, A., Jamieson, B., 2007. Fracture character in compression tests. Cold Reg. Sci. Technol. 47 (1–2), 60–68.

Winkler, K., Schweizer, J., 2009. Comparison of snow stability tests: extended column test, Rutschblock test and compression test. Cold Reg. Sci. Technol. 59, 217–226 (this issue).